

Synthesis of PANI-GO and PANI-rGO nanocomposites and their electrochemical performance

Nisha¹, G. Singh¹, A. Kumar¹, P. Prasher², H. Mudila^{1*}

¹Department of Chemistry, Lovely Professional University, Phagwara, Punjab-144411, India

²Department of Chemistry, UPES, Dehradun, 248007, India

Received: March 27, 2023; Revised: April 30, 2023

In this work, a series of binary nanocomposites (PGs and PGRs) were synthesized by adding a varying percentage of GO and rGO to the matrix of polyaniline (PANI). PANI was synthesized by the chemical oxidative method, while GO was synthesized through the modified Hummers method and was further reduced to rGO. All the individual material and composite materials were analyzed through FTIR, XRD, TGA-DSC, and SEM analysis. The electrochemical performance was studied *via* cyclic voltammetry for the PANI, GO, PGs, and PGRs in the potential range of -0.5 to 0.5 V at varying scans (1 to 500 mV/s). The specific capacitance of PANI, GO, and rGO was found to be 169.57, 248.69, and 279.34 F/g while the maximum specific capacitance for the binary composites for PG-5 and PGR-5 was found to be 367 and 1231 F/g respectively.

Keywords: Polyaniline, Reduced graphene oxide, Electrochemical sensor, Clean energy, Cyclic voltammetry.

INTRODUCTION

Conductive polymers (CPs) are of great interest because of their incomparable properties like high surface area, multi-redox reaction, thermal resistance, and chemical stability. Out of various CPs, polyaniline (PANI) possesses a wide range of electrical properties and is a great choice because of its ease of synthesis [1, 2]. Apart from the CPs, nowadays carbon-containing materials like graphite oxide (GO) and reduced graphite oxide (rGO) provide a capable preliminary material for the fabrication of composites with CPs due to defects and potential functionalization [1, 2]. GO is a single sheet having oxygen-containing functional groups like -OH, C-O-C, and -COOH groups [3] whereas rGO has extraordinary physical and chemical properties, a 2D form of graphite, sp² hybridization, great mechanical properties, electron transport, high surface area, and great conductivity. rGO has a honeycomb-like structure in which one strong bond C-C is present in the plane and another π -bond is present out of the plane having a delocalized network, this structure is important for the availability of electrons for conduction [2, 3]. Numerous improvements have been made to CPs and carbon-containing compounds to form their composites for the reason that they provide low cost, save time, and give a better result of conductivity by acting as electroactive material [4-6].

In this experimental work, systematic studies have been carried out on the fabrication and electrochemical activity of the PANI-GO (PGs) and

PANI-rGO (PGR) composites. The present work involves the formation of a binary composite with different ratios of PANI with GO and rGO (w/w %) by a simple route of *ex-situ* polymerization. The fabricated composites were characterized using FTIR, XRD, TGA, DSC, and SEM. These composites were found to have great electroactive properties when studied for their specific capacitance determined by cyclic voltammetry (CV).

MATERIALS AND METHOD

Materials

Chemicals like aniline ($\rho=1.021$ g/ml, LOBA Chemie), SDS (sodium dodecyl sulfate, Qualikems Fine chem.) ferric chloride (Alpha Chemika), graphite (LOBA Chemie Pvt Ltd), sulfuric acid (Avantor Performance Materials India Ltd), potassium permanganate (Hi-Media Laboratories Pvt. Ltd.), sodium nitrate (Avarice Industries), hydrogen peroxide, hydrochloric acid, hydrazine hydrate and ethanol were procured from LOBA Chemie Pvt Ltd and the chemicals were not further purified because all chemicals were of analytical quality.

Preparation of PANI, GO, and rGO

Preparation of PANI from aniline was carried out by the process mentioned by Bangade *et al.* 2020, in the presence of an anionic surfactant and an oxidant FeCl₃ [7]. GO was formed by the modified Hummers method as explained by Mudila *et al.* 2014 [8]. In a beaker deionized water (250 ml) was taken to which

* To whom all correspondence should be sent:
E-mail: harismudila@gmail.com

2g of GO was added and was subjected to stirring over a magnetic stirrer (1100 rpm). Then 2 ml of hydrazine hydrate was dropwise added to the above solution. The mixture was heated at 80 °C for 72 hours with continuous stirring. Fine black particles were observed after the reaction completion which were separated by centrifugation (~5000 rpm).

Fabrication of binary composites PANI-GO (PGs) and PANI-rGO (PGRs)

Six compositions (PGs) of PANI and GO were prepared by varying the amount of GO in the matrix of PANI (Table 1). The requisite amounts of PANI and GO were mixed (*ex-situ* method) in ethanol and were further sonicated in a bath sonicator for 1 hour for better mixing. The composites obtained were then dried in a vacuum oven [6]. The same method was used to prepare the binary composite of PANI-rGO.

Table 1. Composition, ratio, and code for PANI-GO composites

PANI	0.1 g	0.1 g	0.1 g	0.1 g	0.1 g	0.1 g
GO	0.025 g	0.05g	0.075g	0.1 g	0.2g	0.3 g
Ratio	4:1	2:1	4:3	1:1	1:2	1:3
Code	PG-1	PG-2	PG-3	PG-4	PG-5	PG-6

Table 2. Composition, ratio, and code for PANI-rGO composites

PANI	0.1 g	0.1 g	0.1 g	0.1 g	0.1 g	0.1 g
rGO	0.025 g	0.05 g	0.075 g	0.1 g	0.2 g	0.3 g
Ratio	4:1	2:1	4:3	1:1	1:2	1:3
Code	PGR-1	PGR-2	PGR-3	PGR-4	PGR-5	PGR-6

Electrode preparation

The working electrode was prepared of stainless steel(304-SS) which was de-greased by acetone. The material to be coated over the SS electrode was containing 0.05 g of electroactive material added with graphite (0.005 g) in a binder polystyrene (5 g/dL in xylene). The material was dried and weighted (~ 0.01 g) and was further used as a working electrode in 1M KOH solution [8]. The electrochemical measurement of PANI, GO, rGO, PANI-GO, and PANI-rGO was done by cyclic voltammetry (CV) in a -0.5 to 0.5V potential window range at a scan rate of 1 to 500 mV. The specific capacitance (C_s) of the active materials calculated from the cyclic voltammograms curves is given by the equation.

$$C_s = A/2mk.\Delta V$$

where, A= area under the CV curve, m= mass loaded of the electro-active material, k=applied scan rate (1 to 500 mV/s), ΔV =applied potential window -(0.5 to 0.5 V).

RESULTS AND DISCUSSION

Electrochemical measurement

Electrochemical performance of PANI, GO, and rGO. Fig. 1. shows the electrochemical behavior of

PANI, GO, and rGO. Specific capacitance values increase progressively from PANI to GO and rGO due to their structural property which possesses the availability of free electrons for electric conduction, this may be attributed to the increased surface area and porous structure of all the materials. CV curves show a regular increase in the range of cathodic and anodic current with enhanced scan rate but this trend was not continuous and led to a decrease in specific capacitance indicating the stability of the materials. Table 3 depicts the C_s values of PANI, GO, and rGO at various scan rates with the highest capacitance value of 169.5, 248.69, and 279.34 F/g, respectively at 1 mV/s and the values decreases regularly as the scan rate increases from 1 to 500 mV/s [6, 8].

Table 3. Specific capacitance of PANI, GO, and rGO at different scans

Scan Rate	Specific capacitance (C_s) F/g		
	PANI	GO	rGO
1mV/s	169.5	248.69	279.34
5mV/s	50.77	100.46	72.50
10mV/s	32.60	73.89	46.60
50mV/s	10.79	38.32	19.60
100mV/s	6.40	27.18	13.07
500mV/s	2.58	11.04	5.05

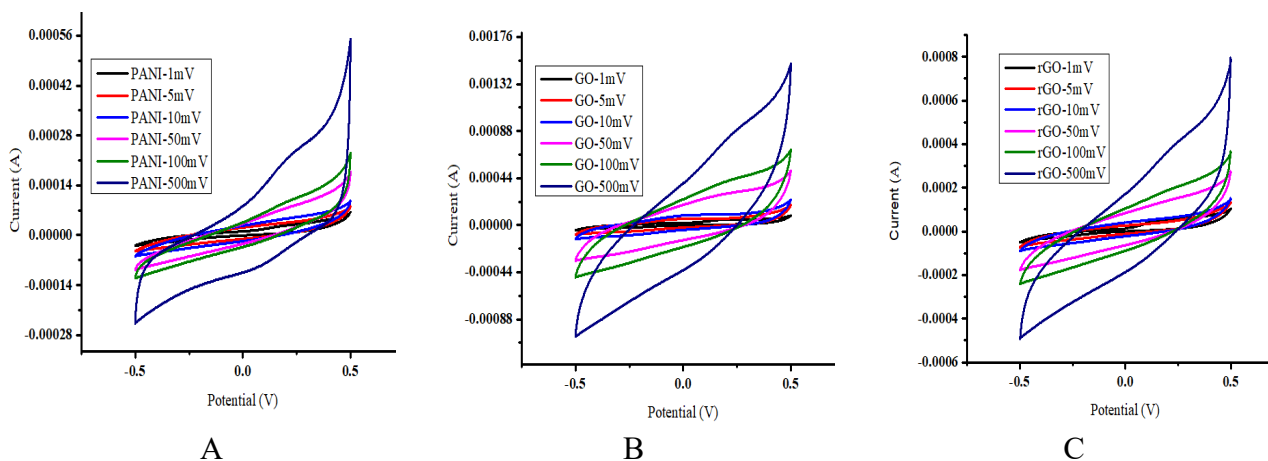


Figure 1. Cyclic voltammogram of (A) PANI (B) GO (C) rGO at different scan rate

Table 4. Specific capacitance of PGs at different scans rates

Scan rate	Specific capacitance (C_s) F/g					
	PG-1	PG-2	PG-3	PG-4	PG-5	PG-6
1mV/s	85.32	95.6	161.0	210.0	367.0	181.0
5mV/s	15.13	69.3	46.96	46.08	132.54	66.03
10mV/s	11.8	48.1	23.48	24.57	96.52	40.5
50mV/s	4.29	22.9	10.8	11.26	47.39	23.87
100mV/s	3.04	16.2	6.3	8.4	34.08	16.89
500mV/s	1.7	6.9	4.8	4.8	15.7	5.8

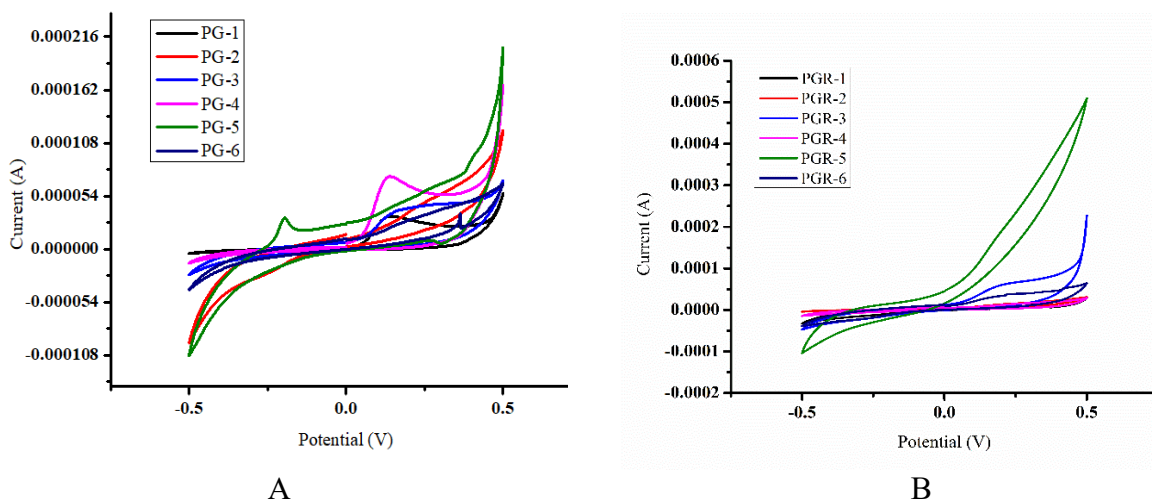


Figure 2. Comparative cyclic voltammogram of (A) PGs all ratios at 1mV/s (B) PGRs all ratios at 1mV/s

Table 5. Specific capacitance of PGRs at different scans rates

Scan rate	Specific capacitance (C_s) F/g					
	PGR-1	PGR-2	PGR-3	PGR-4	PGR-5	PGR-6
1mV/s	102.0	226.2	305.2	323.4	1231.9	310
5mV/s	24.5	155.7	76.6	56.7	305.8	105.2
10mV/s	14.8	122.1	49.3	43.7	73.2	69.3
50mV/s	12.7	53.9	23.1	22.3	61.2	34
100mV/s	9.3	37.1	39.9	16	38.4	25.8
500mV/s	4.4	14.4	8.5	6.8	14.1	13.5

Electrochemical performance of binary composites PGs and PGRs

The specific capacitance of PANI increases with the addition of specific weight percentages of GO and rGO because they get homogeneously grafted on the PANI matrix and surface area gets enhanced, but this increase was not regular (Tables 4, 5). The maximum value of C_s was achieved for PG-5 (367 F/g) and PGR-5 (1231.9 F/g), afterward, there is a decrease in C_s due to more addition of GO and rGO layers on PANI inhibiting the conduction and reducing the active surface area. Well-aligned PGs and PGRs show excellent performance as electrode materials. Maximum C_s values of PGR-5 as compared to PG-5 were shown for the reason that it facilitates electrolyte diffusion in the honeycomb-like carbon structure (more available in PGR) and π -bond that is present out of the plane having a delocalized network, this structure is important for the availability of electrons for conduction [2]. Fig. 2 shows the voltammogram of PGs and PGRs in all ratios at 1mV/s.

Fig. 3 depicts that the binary composite in the ratio PG-5 (1:2) and PGR-5 (1:2) was found to have the highest C_s .

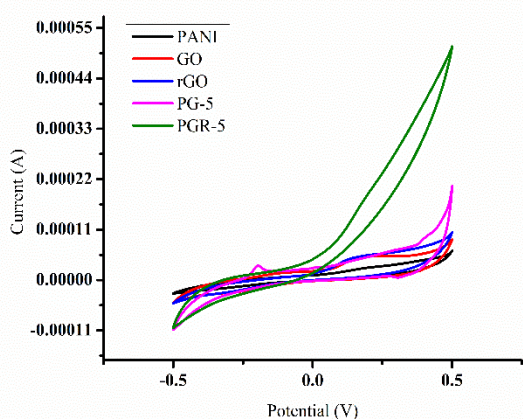


Figure 3. Cyclic voltammograms of PANI, GO, rGO, PG-5 and PGR-5

The slope, as well as the area of the CV curve of PGR-5 and PG-5 is higher than PANI, GO, and rGO

signifying the reduced resistance, fast ion diffusion rate, and good capacitance behavior in composite material. As a result, the CV dimensions of the composite 1:2 shows the utmost current and reveal a large surface area of CV curves indicating the enhanced specific capacitance attributed to synergic consequence among GO and PANI matrix as well as rGO and PANI matrix [18].

Fourier transform infrared (FTIR)

The powdered samples (PANI, GO, rGO, PG, and PGR) were characterized by using FTIR (Perkin Elmer Spectrum IR Version 10.6.1). PANI showed characteristic peaks at 3412, 2978, 1549, 1450, 1293, 1230, 1036, and 783 cm^{-1} corresponding to N-H str., C-H str., C=C bond, benzenoid ring, C-N bond, N-H bend., C-H bend., and quinoid ring respectively [10, 11]. The peaks at 3164, 1712, 1618, and 1039 cm^{-1} were the characteristic peaks of O-H stretching, C=O stretching, C=C bond, and C-O stretching of graphene oxide (GO) [12, 13]. rGO showed peaks at 1544, 3389, and 1709 cm^{-1} for skeletal vibrations, -OH stretching and C=O stretching [14] as shown in Figure 4. The peaks at 1711, 1560, 1107, and 799 cm^{-1} correspond to the C=O stretching, N-H bending, C-H stretching of the benzenoid ring, and C-H out-of-plane bending vibrations in binary composite PG [15, 16]. Another binary composite PGR showed peaks at 1708, 1453, 1292, and 1096 cm^{-1} owing to the presence of the C=O group, C=C str. of benzenoid rings, and C-N bend. of the benzenoid ring, and C-H stretching of the quinoid ring [17, 18] as shown in Figure 4.

X-ray diffraction (XRD)

The XRD of all samples was studied by using an X-ray diffractometer (Bruker D8 advance) using $\text{Cu-K}\alpha$ radiation. The broad peak at about $2\theta = 25^\circ$ is the characteristic peak of PANI [26]. The characteristic peak of the graphite $2\theta = 26.4^\circ$ (Fig 5A) was transformed to $2\theta = 10.61^\circ$ (Figure 5B) when converted to GO, which was attributed to the presence of oxygenated groups and water molecules inserted in the interlayer of graphite. For rGO samples weak broad peak at approximately $2\theta = 24.5^\circ$ is observed (Fig 5B) [13].

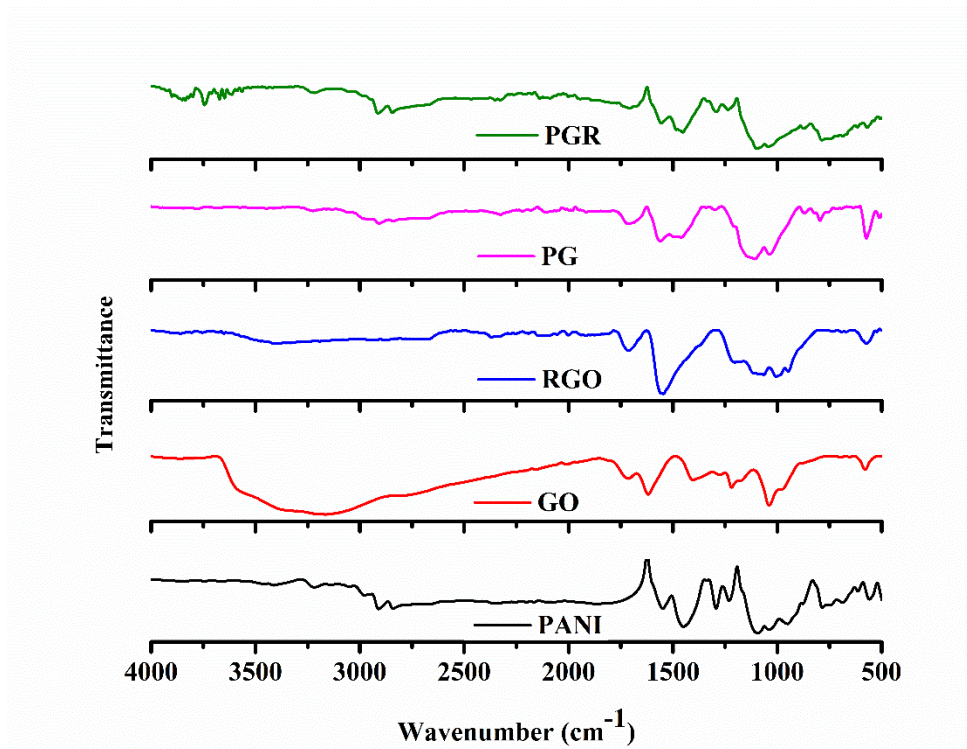


Figure 4. FTIR spectra of all the individual materials and composites

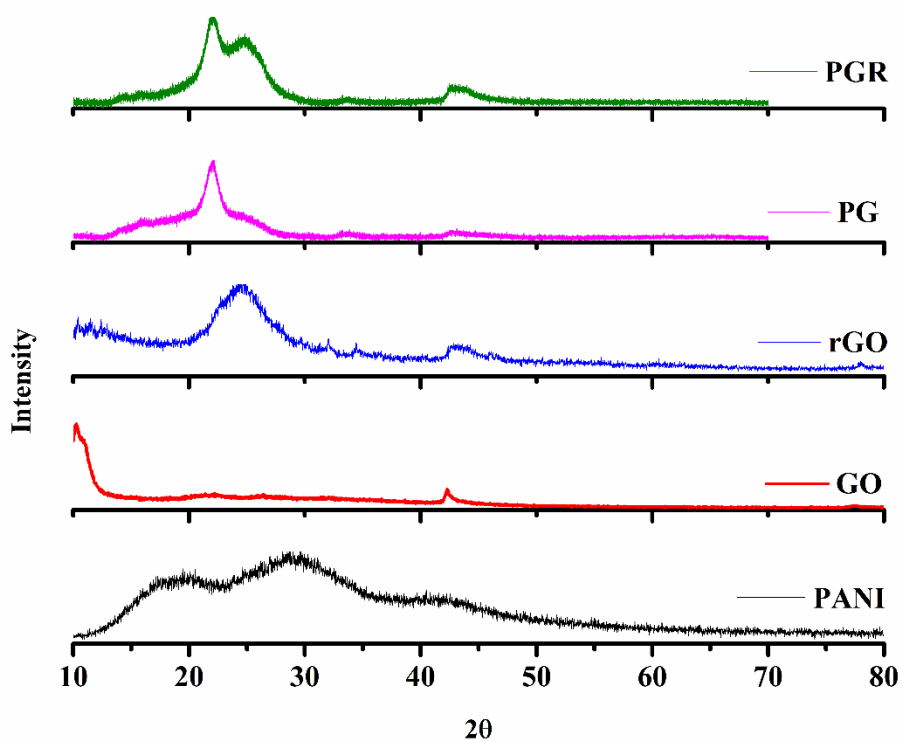


Figure 5. XRD of all individual materials and composites

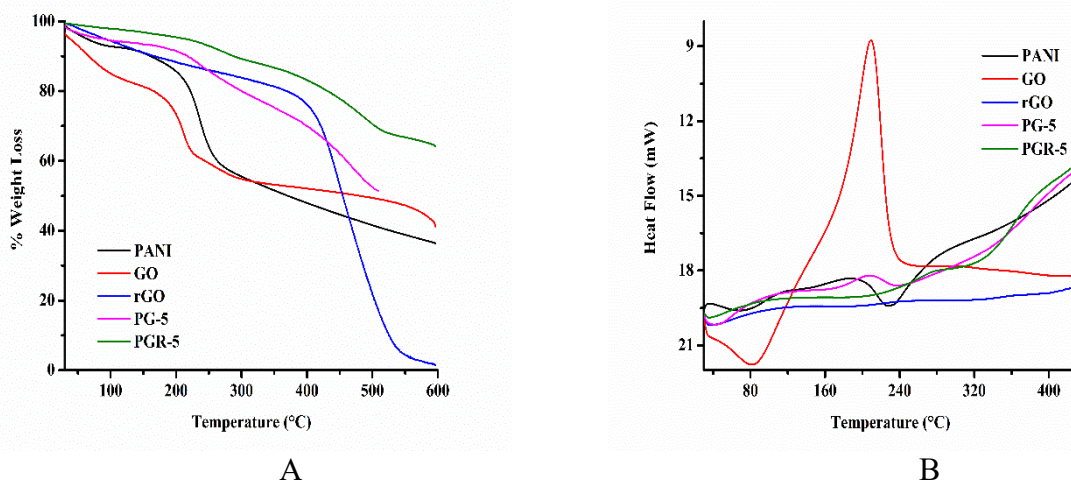


Figure 6. (A) TGA and (B) DSC of individual and composite materials

Thermogravimetric analysis (TGA)

TGA was executed to predict the thermal stability of a material, the data was recorded on the instrument (TGA)-50H of Perkin Elmer. A material of the weight (x mg) was heated under an inert (N_2) atmosphere with a flow of 10 °C/min (room temperature to 600 °C) to record the TG data. For PANI a three-step weight loss was observed, and two minima were depicted which are due to weight loss. The first weight loss is due to the loss of adsorbed water at 100 °C and the second weight loss of 27 % is due to the decomposition of PANI between 100 °C to 300 °C. The third weight loss of 12 % started above 300 °C due to the degradation of the polymeric backbone of PANI [19].

For GO the TGA plot shows that the weight loss (%w) occurred in three steps, initially a mass loss (20 %) occurred below the temperature of 117 °C because of the removal of the water absorbed. In the 2nd step, mass loss (30 %) occurs up to the temperature of 200 °C due to the thermal decomposition of functional groups containing oxygen ($-OH$, $-COOH$, etc.) to yield CO , and CO_2 [20]. It was observed that there was smaller weight loss taking place in rGO as compared to GO, which is by reason of the presence of less percentage of groups like $-OH$, $-COOH$, etc. in rGO [21]. It has been observed that the percentage mass loss of PG is nearly positioned at the weight loss range of individual components Go and PANI, however, the weight loss curve of PG was somewhat closer to GO indicating the stability of PG. Thus, it can be inferred that PANI has been successfully grafted on the surface of GO [22]. The composite PGR below 150 °C showed a minute weight loss suggesting low moisture absorbed by the sample. Maximum weight loss occurred at a temperature range of 200 to 300 °C

and weight loss at approx. 550 °C was due to the probable decomposition of rGO [23]. The comparative TGA of individual materials and their binary composite has been shown in Fig. 6 A.

Differential scanning calorimetry (DSC)

DSC is a very successful technique to determine the heat flow in the sample by using a DSC analyzer 50H of Perkin Elmer. A material of the known weight was heated under an inert (N_2) atmosphere at a 10 °C/min flow rate (from room temperature to 500 °C) to record the DSC data. DSC of PANI showed endothermic peaks at a lower temperature due to loss of water molecules and another endothermic peak was observed due to the decomposition of amine units as depicted by TGA results also. The endothermic peak below 100 °C was related to the evaporation of water molecules and the 2nd endothermic peak was observed at 230 °C due to the decomposition of the dopant, while the exothermic peak at 431 °C accounted for the breakdown of PANI backbone [24]. In GO the endothermic peak below 100 °C indicates evaporation of water molecules and also signifies that the de-oxygenation reaction starts below this temperature. A peak at 212 °C (endothermic) corresponds to the breakdown of oxygenated functional groups ($-OH$ and $-COOH$ etc.) with the evolution of CO and CO_2 [20]. In the case of rGO due to absorbed moisture an endothermic peak (below 100 °C) due was encountered, also an exothermic peak near 200 °C was observed due to the loss of oxygenated functional groups. However, these peaks were less intense as compared to the peaks observed in GO due to a smaller number of $-OH$ and $-COOH$ gr. The reduction of GO into rGO results in a decline in the number of functional groups, hence peak intensity

decreases [25]. In the presence of GO, and PANI there is a cross-linking reaction that results in thermodynamically destitute at lower temperatures. The binary composite showed an endothermic peak below 100 °C owing to the loss of moisture, an exothermic peak (209°C) due to the release of certain gases, and an exothermic peak at 433 °C due to the breakdown of the backbone of the polymer, which signifies the successful formation of the binary composite. Another binary composite PANI-rGO (PGR-5) shows an endothermic peak at 107 °C and two exothermic peaks, one at 278°C and the second at 435 °C. The peak intensity was found to be lower in binary composite because of enhancement in thermal stability [26, 27] as shown in Fig. 6B.

Scanning electron microscopy (SEM)

SEM image shows the average size of nanoparticles of PANI was about 60 nm [28]. These micrographs confirm the approximately spherical shape of the nanoparticles. In GO numerous folded and wrinkled sheet-like structures can be easily seen, and the GO presented a randomly arranged structure. SEM images of rGO showed that the wrinkled and folded sheets present in GO were reduced and were changed to exfoliated sheet-like appearance which might lead to a better exfoliated surface area thus leading to better electron navigation [29]. PANI was homogeneously surrounded by GO fibers in binary composite PG [27]. PGR composites show that the PANI nanoparticles lie on the RGO's surface [17].

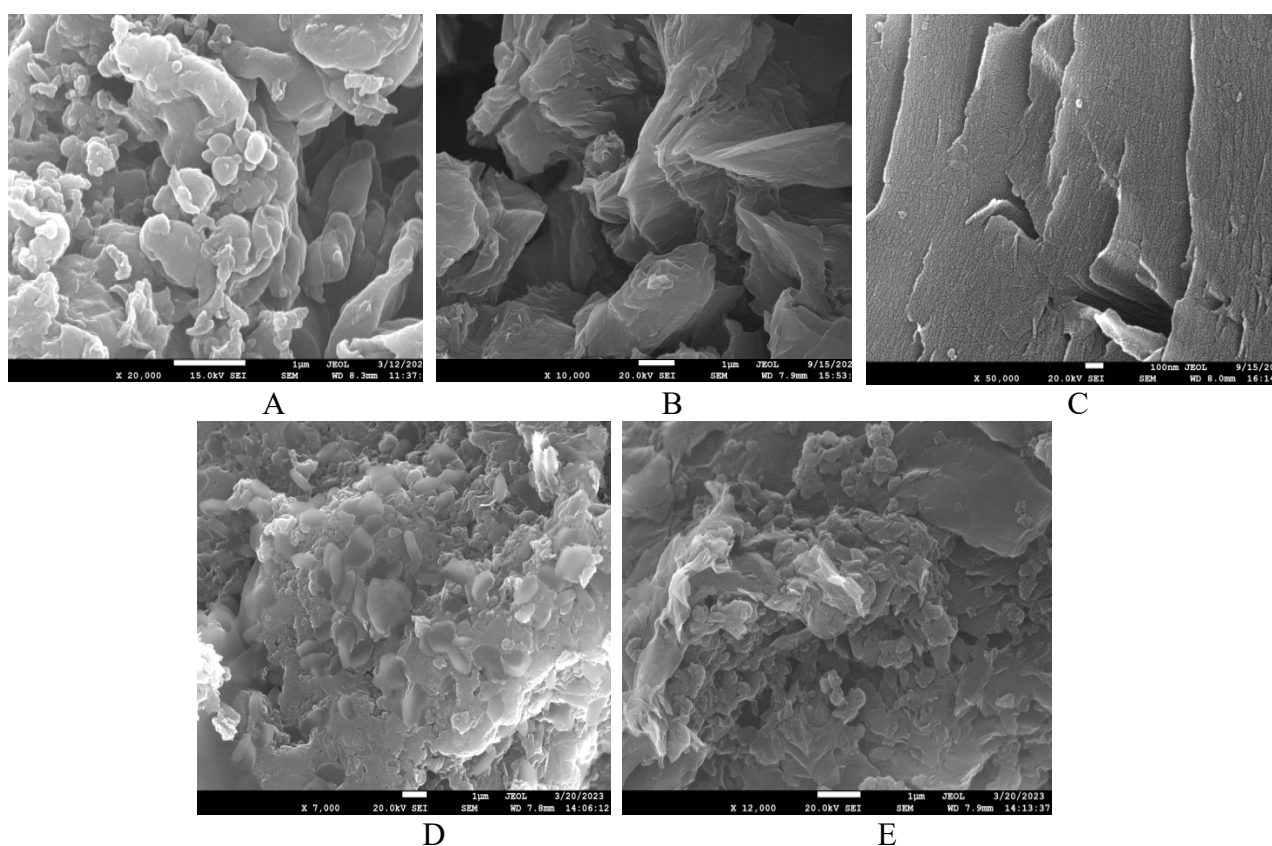


Figure 7. SEM micrographs of (A) PANI (B) GO (C) rGO (D) PG-5 and (E) PGR-5

CONCLUSION

A series of binary nanocomposites of PANI with GO (PG) and rGO (PGR) were successfully prepared via the *ex-situ* method in various ratios. These binary composites were compared for their electrochemical behavior by studying their associated specific capacitance measured by cyclic voltammetry. The results show a maximum specific capacitance of 169.5, 248.5, and 279.34 F/g for PANI, GO, and rGO at 1 mV/s. In the binary composition, the PG-5 has a ratio of 1:2 and was found to have the greatest C_s of 367 F/g, while 1231.9 F/g was the maximum

capacitance of PGR-5 nanocomposite with a 1:2 ratio. Further, the fabricated nanocomposites (PG and PGR) and individual materials (PANI, GO, and rGO) were analyzed by FTIR, XRD, SEM, TGA, and DSC for their chemical, structural and thermal characteristics.

Conflicts of interest: No conflicts of interest are declared by the authors.

REFERENCES

1. T. N. A. B. T. A. Mutalib, S. J. Tan, K.L. Foo, Y. M. Liew, C. Y. Heah, M.M.A.B. Abdullah. *Pol. Bull.*, **78**, 4835 (2020), doi:10.1007/s00289-020-03334-w
2. D. George, G. James, J.K. Manjally, J. Thomas, M.S. Kuriakose, K.S. Aryamol, S.C. George. Application. *Mater. Today: Proc.*, **24**, 1734 (2020), doi:10.1016/j.matpr.2020.03.597
3. G. Xu, N. Wang, J. Wei, L. Lv, J. Zhang, Z. Chen, Q. Xu. *Ind. Eng. Chem. Res.*, **51**, 14390 (2012), doi:10.1021/ie301734f
4. M. Ates M. Yildirim. *Pol. Bull.*, **77**, 2285 (2019), doi:10.1007/s00289-019-02850-8
5. F. Soysal, Z. Çıplak, B. Getiren, C. Gökalp N. Yıldız. *Mat. Res. Bull.*, **124**, 110763 (2020), doi:10.1016/j.materresbull.2019.110763
6. Shruthi, K.M. Vighnesha, Sandhya, D.N. Sangeetha M. Selvakumar, *Surf. Eng. Appl. Electrochem.*, **54**, 359 (2018), doi:10.3103/s106837551804018x
7. S.S. Bangade, V.M. Raut, S.E. Bhandarkar D.P. Gulwade. *Mater. Today: Proc.*, **29** (2020), doi:10.1016/j.matpr.2020.04.790
8. H. Mudila, V. Joshi, S. Rana, M.G.H. Zaidi S. Alam . *Carbon Lett.*, **15**, 171 (2014), doi: 10.5714/CL.2014.15.3.171
9. H.Mudila, M.G.H. Zaidi, S. Rana, V.Joshi, S. Alam. *Int. J. Chem. Anal. Sci.*, **4**, 139 (2013), doi:10.1016/j.ijcas.2013.09.001
10. B. Butoi, A. Groza, P. Dinca, A. Balan V. Barna, V. *Polymers.*, **9**, 732 (2017), doi: 10.3390/polym9120732.
11. B.S. Singer, S. Palaniappan, S. Pabba. *J. Electrochem. Soc.*, **159** (2020), doi: 10.1149/2.036201jes
12. S. Drewniak, R. Muzyka, A. Stolarezky, T. Pustelny, T.M.K. Moranska M. Setkiewicz. *Sensors.*, **16**, 103 (2016), doi: 10.3390/s16010103
13. X. Jiao, Y. Qiu, L. Zhang and X. Zhang. *RSC Adv.*, **7**, 52337 (2017), doi:10.1039/c7ra10809e
14. F.T. Thema, M.J. Moloto, E.D. Dikio, N.N. Nyangive, L. Kotsedi, M. Mazza M. Khenfouch. *J. Chem.*, **2013**, 150536 (2013), doi: 10.1155/2013/150536
15. M. Manoj, K.M.A. kumar, B. Jinisha S. Jayalekshmi. *J Mater Sci Mater Electron*, **28**, 14323 (2017), doi:10.1007/s10854-017-7292-9
16. M. Mahadik, H. Patil, G. Bodkhe, N. Ingle, P. Sayyad, T. A. Gahaouri, S. M. Shirsat, M. Shirsat. *Front. Mater.*, **7** (2020), doi: 10.3389/fmats.2020.00081
17. Y. Zhang, J. Liu, Y. Zhang, J. Liu Y. Duan. *RSC Adv.*, **7**, 54031 (2017), doi:10.1039/c7ra08794b
18. S. Palsaniya, H. B. Nemade, A. K. Dasmahapatra. *J Phys. Chem. Solids*, **154**, 110081 (2021), doi:10.1016/j.jpcs.2021.110081
19. A. Kumar, A. Kumar, H. Mudila, K. Awasthi V. Kumar. *J. Phys.*, **1531** (2020), doi:10.1088/1742-6596/1531/1/012108
20. S.N. Alam, N. Sharma, L. Kumar, L. *Graphene.*, **6** (2017), doi: 10.4236/graphene.2017.61001
21. N. Sharma, V. Sharma, Y. Jain, M. Kumari, R. Gupta, S, K. Sharma K. Sachdev *Macromol. Symp.*, **376**, 1700006 (2017), doi:10.1002/masy.201700006
22. Q. Fan, Y. Yang, Y. Hao, X. Zhao Y. Feng. *J. Mol. Liq.*, **212**, 557, (2015), doi:10.1016/j.molliq.2015.10.008
23. Y. Wang, X. Wu, W. Zhang S. Huang. *Syn. Metals*, **210**, 165 (2015), doi:10.1016/j.synthmet.2015.09.022
24. M. Matoetoe, F. Okumu, C. Maphale O. Fatoki. *Asian J. Chem.*, **27**, 1411 (2015), doi:10.14233/ajchem.2015.18061
25. J. Singh A.S. Dhaliwal (2022). *J. Phys Chem Solids.*, **160**, 110358 (2022), doi:10.1016/j.jpcs.2021.110358
26. A. L. Ahmad, U. R. Farooqui, N. A. Hamid, *RSC Adv.*, **8**, 25725 (2018), doi:10.1039/c8ra03918f
27. L.R. Vargas, A.K.D.S. Poli, R. de C.L. Dutra, C. B. De Souza, M.R. Baldan E.S. Gonçalves. *J. Aerosp. Technol. Manag.*, **9**, 29 (2017), doi:10.5028/jatm.v9i1.697
28. A. Abdelrahmeen M.F. Elkady. *Alex. Engg J.*, **57**, 3291 (2018), 10.1016/j.aej.2018.01.012
29. B. Thirumalraj, C. Rajkumar, S.M. Chen S. Palanisamy. *Sci. Rep.*, **7** 41213 (2017), doi:10.1038/srep4121